Here, the analysis is restricted to a region near the orifice where $s \simeq z$, or to the lowest order

$$\frac{dz}{dt} = u_o \tag{A5}$$

and

$$\frac{dz}{dt} = \frac{1}{2}\left(\frac{l_m}{x}\right)^{1/2}\left(\frac{1/2}{\alpha + \beta/R}\right)^{1/2}\frac{dx}{dt} \tag{A6}$$

from Equation (16) where x, z refer to the coordinates of a fluid parcel within the jet. Letting $K = 2^{1/2}(\alpha + \beta/R)^{1/2}$ where $K = 0(1)$ for all R and combining Equations (A5) and (A6), one has

$$\frac{1}{v}\frac{dx}{dt} = 2KR\left(\frac{x}{l_m}\right)^{1/2} \tag{A7}$$

From Equation (A7) it is seen that a parcel of fluid within the jet will equilibrate with the ambient fluid when $1/v\ dx/dt \rightarrow 1$, or at

$$x_e = \frac{l_m}{4K^2R^2} \quad \text{for} \quad R > 1.0 \tag{A8}$$

This occurs in a travel time t_e, where

$$t_e = \frac{1}{v}\left(\frac{l_m^{1/2}}{2KR}\right)\int_0^{x_e}\frac{dx}{x^{1/2}} \tag{A9}$$

by the integration of Equation (A7). Thus the equilibration time is

$$t_e = \frac{1}{2vK^2}\left(\frac{l_m}{R^2}\right) \quad \text{for} \quad R > 1.0 \tag{A10}$$

or the total travel distance of the fluid parcel at the end of the near field when $t = \omega^{-1}$ is

$$x = x_e + v(\omega^{-1} - t_e) \tag{A11}$$

where $v/\omega = l_D$. Substitution of Equations (A8) and (A10) into Equation (A11) gives, with some rearrangement

$$\frac{x}{l_D} = 1 - \left(\frac{1}{4K^2}\right)\left(\frac{l_m}{l_D}\right)\left(\frac{1}{R^2}\right)$$

$$\text{at} \quad t = \omega^{-1} \quad \text{and} \quad R > 1.0 \tag{A12}$$

where $1 < 2K < 2.4$ and $l_D/l_m = 0(1)$ for $1 < R < \infty$. Thus, the assumption that jet fluid parcels near the orifice travel a distance equal to that of the ambient fluid for times on the order of ω^{-1} appears to be a reasonable one.

Manuscript received October 23, 1978; revision received March 2, and accepted March 26, 1979.

Surface Ablation in the Impingement Region of a Liquid Jet

MICHAEL J. SWEDISH
MICHAEL EPSTEIN
JOHN H. LINEHAN
GEORGE A. LAMBERT
GEORGE M. HAUSER
and
LARRY J. STACHYRA

Argonne National Laboratory
9700 South Cass Avenue
Argonne, Illinois 60439

A theoretical and experimental investigation of a water jet impinging on a melting solid surface has been carried out. Ice, octane, *p*-xylene, and olive oil served as the meltable solid materials, comprising a Prandtl number range of 5 to 2 800. An available laminar stagnation flow model was utilized to describe melting heat transfer in the jet impingement region. Melting rate measurements were found to agree quite well with the values predicted with this model.

SCOPE

Fluid jets impinging on surfaces result in high rates of heat transfer as compared with most other forced convection flow geometries. This fact has led to the recent application of hot liquid or gaseous jets to drill through solid material (Mellor, 1974). An important feature of the flow in this application is the insulating effect of the thin layer of melt which forms between the impinging jet and the melting solid. Melting in the impingement region of a fluid jet is also important in other practical situations; for example, the aerospace industry relies on meltable materials to relieve aerodynamic heating in the stagnation region of spacecraft requiring atmospheric entry; the integrity of protective steel barriers when subjected to jets of molten reactor material is an important safety question in current design of in-pile experiments that attempt to simulate postulated core disruptive accidents for the fast breeder reactor; and melting can be exploited to delineate heat transfer rates for liquid jets impinging on nonmelting surfaces.

While many studies have been reported on the heat and mass transfer characteristics of impinging fluid jets, the attention of researchers has overwhelmingly remained focused on gas jets. Relatively little work has been reported on the heat transfer between a liquid jet and the surface on which it impinges. Sitharamayya and Subba Raju (1969) performed the only experimental study of heat transfer between a submerged liquid (water) jet and a flat solid surface held normal to the flow. Yen and Zehnder (1973) studied ablation of ice by a liquid (water)

Correspondence concerning this paper should be addressed to Michael Epstein. Michael J. Swedish is with Wisconsin Electric Power Company, Milwaukee, Wisconsin. John H. Linehan is with Marquette University, Milwaukee, Wisconsin.

jet emanating from a nozzle into air (free liquid jet). Their work, which was largely experimental, involved formation of a cavity in a block of ice, which resulted in a nonflat impingement surface and, therefore, a complex flow geometry. Gilpin (1973) performed similar experiments. An experimental study by Savino et al. (1970), in which a submerged water jet was directed against a cold surface, was concerned with a liquid solidifying on or melting its own solid.

Roberts (1958) carried out one of the first theoretical studies of impingement heat transfer with melting. His approximate solution to the governing conservation equations for laminar fluid motion in the neighborhood of a stagnation point, including both the jet region and the melt film, was applied to the melting of a body of ice by a hot stream of air; however, the formulation was general and could be extended to higher density jets without difficulty. A theoretical analysis for a liquid jet impinging on a melting surface of the same material was made by Lipsett and Gilpin (1978). Their work included analysis in both the stagnation region and the wall jet region downstream of the stagnation region. The transient problem of the formation of a frozen layer in plane stagnation flow was studied analytically by Yang (1966).

The objective of the present investigation was to obtain experimental data on the melting rates produced by the impingement of an axisymmetric liquid jet on a melting solid surface. The impinging liquid and the melting solid may be two different materials of immiscible liquids. Our measurements were directed towards the determination of the resistance to melting heat transfer due to the immiscible melt layer. To the best of the present authors' knowledge, such data are unavailable.

In order to maintain a flat impingement surface during the melting process, a water jet was directed upward against the lower end of a meltable rod having a diameter about twice that of the nozzle used to produce the jet. Melting data have been collected for water impinging on ice (one-component system) and for water impinging on solid octane (C_8H_{18}; m.p. -56.8°C), *p*-xylene (1,4 dimethylbenzene; m.p. 13.2°C), and olive oil (m.p. -6.0°C), corresponding to a two-component system. The melting heat transfer data has been correlated successfully by adopting the laminar two-fluid model proposed by Roberts (1958).

CONCLUSIONS AND SIGNIFICANCE

The rate of ablation of a low melting point solid when subjected to a hot, free liquid jet of normal incidence was examined analytically and experimentally. Attention was focused on the stagnation region of an axisymmetric jet. The impinging liquid and the melting solid may be the same material or two different materials where the liquids are immiscible. The following important results were obtained:

1. Despite the fact that the jet flow is highly turbulent as it exits the nozzle, the experimental data indicate that a melt layer is always present and insulates the melting surface from the impinging jet.

2. A laminar, two-fluid, stagnation flow model successfully predicts melting rates in the vicinity of the stagnation point, even though the jet is turbulent. Moreover, an approximate analytic solution which treats the melt layer as a thin film can be most useful in predicting melting rates over a range of jet velocities and temperatures which are of practical interest.

3. Melting rate measurements can be used to determine jet impingement heat transfer to a nonmelting surface. In this application, the melting technique is more straightforward than corresponding nonmelting techniques for measuring heat transfer rates.

PHYSICAL MODEL

The jet impingement heat transfer at a melting surface will be analyzed according to Roberts (1958) description of the steady melting of ice in an impingement flow of warm air but with an extension to higher density (liquid) jets. In particular, we consider the neighborhood of the stagnation point of an axisymmetric liquid jet impinging on a melting solid surface. The impinging liquid and the melting solid may be the same material or two different materials of immiscible liquids.

A schematic diagram of the physical model of the subject phenomena is presented in Figure 1. The jet is separated from the solid in the impingement region by a constant thickness film of melted material. The coordinate system is fixed to the solid film interface so that, under steady state conditions, the interior of the melting solid moves toward the stationary melting surface at a constant velocity equal to the melting velocity. This choice of coordinate system corresponds exactly to the physical experiments described below. The physical properties that appear in the governing equations are considered to be constant.

Calculation of the nozzle Reynolds number for the experiments reported here indicates that the oncoming jet is turbulent. Available data and analysis for turbulent air jets suggest that for impingement close to the stagnation point, the heat (or mass) transfer can be computed by applying turbulent correction factors to the laminar values (Donaldson et al., 1971; Giralt et al., 1977). The correction factors have been found to be only a function of the axial nozzle orifice to impingement surface distance and not a function of jet Reynolds number. For nozzle to surface distances less than four nozzle diameters, it was concluded that significant penetration of turbulence into the boundary layer near the surface does not occur, as there is good agreement between laminar predictions and measured rates. For larger axial distances, turbulence in the impinging jet is high, and laminar predictions fall below measured values. This behavior leads one to suspect that the initial nozzle induced turbulence does not affect the rate of heat transfer, but, instead, it is the interaction of the air jet with the surrounding atmosphere that causes the increased heat transfer rates. In view of this and the fact that the interaction between a liquid jet and its surrounding air

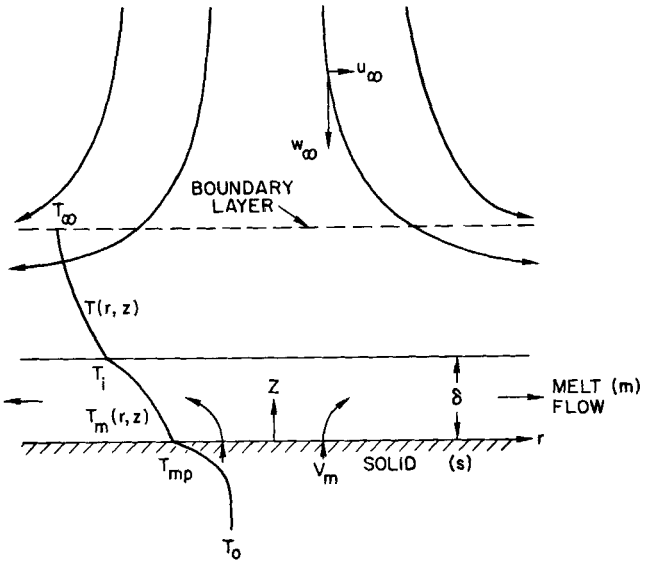

Fig. 1. Schematic diagram of jet impingement on a melting surface indicating temperature profile and nomenclature.

atmosphere is so much less than that for an air jet, it is unlikely that the turbulence correction factor is required for a liquid jet. The present model, therefore, deals only with the laminar equations in the stagnation region.

Owing to the finite diameter of the liquid jet in the experimental flow, the axisymmetric stagnation flow model breaks down at a certain distance r from the stagnation point. According to measurements made with gas jets impinging on solid surfaces, the limiting distance r is about 1.2 times the jet (or nozzle) diameter d (see Martin, 1977, for a summary of this work). Our analysis will be restricted to this distance.

Our two-fluid model requires that the jet-melt film interface is stable to displacement perturbations. Recently, Erickson and Olfe (1978) demonstrated that an instability of the Kelvin-Helmholtz type is bounded in the stagnation counterflow illustrated in Figure 1.

GOVERNING EQUATIONS

The governing partial differential equation for a steady state, laminar, axisymmetric stagnation flow with heat transfer can be found in standard heat transfer or fluid flow textbooks, and it is not necessary to repeat them here. The pertinent boundary conditions are

$$\text{at } z \to \infty: \quad u \to u_\infty = ar, \quad w \to w_\infty = -2az, \quad T \to T_\infty \tag{1}$$

$$P \to P_\infty = P_0 - \tfrac{1}{2}\, a^2\rho(r^2 + 4z^2) \tag{2}$$

$$\text{at } z = 0: \quad u_m = 0, \quad w_m = V_m, \quad T_m = T_{mp} \tag{3}$$

$$k_m \frac{\partial T_m}{\partial z} = [L + C_s(T_{mp} - T_0)]\rho_m V_m \tag{4}$$

$$\text{at } z = \delta: \quad u = u_m, \quad w = w_m = 0, \quad T = T_m = T_i \tag{5}$$

$$\mu \frac{\partial u}{\partial z} = \mu_m \frac{\partial u_m}{\partial z}, \quad k \frac{\partial T}{\partial z} = k_m \frac{\partial T_m}{\partial z} \tag{6}$$

Note that unsubscripted properties and variables pertain to that part of the flow which is in the jet ($\delta < z < \infty$), while those in the film region ($0 < z < \delta$) bear the subscript m. In Equations (1) and (2), a is the stagnation point velocity gradient. It has been found experimentally that $a \simeq w_\infty/d$, where d is the diameter of the nozzle from which the jet emerges (see Martin, 1977, for a summary of this work).

It is well known that the governing partial differential equations can be reduced to a system of ordinary differential equations by introducing the following transformed variables:

$$\eta = \sqrt{\frac{2a}{\nu}}\, z, \quad u = ar\frac{df(\eta)}{d\eta}, \quad w = -\sqrt{2a\nu}\, f(\eta) \tag{7}$$

$$P = P_0 - \tfrac{1}{2}\,\rho a^2\left[r^2 + \frac{\nu}{a}F(\eta)\right] \tag{8}$$

for the jet region, and

$$\eta_m = \sqrt{\frac{2a_m}{\nu}}\, z, \quad u_m = a_m r \frac{df_m(\eta_m)}{d\eta_m}, \quad w_m = -\sqrt{2a_m\nu_m}\, f_m(\eta_m) \tag{9}$$

$$P_m = P_0 - \tfrac{1}{2}\,\rho_m a_m^2\left[r^2 + \frac{\nu_m}{a_m}F_m(\eta_m)\right] \tag{10}$$

for the melt region. The stagnation point velocity gradient a_m for the melt flow is related to a according to

$$a_m = \left(\frac{\rho}{\rho_m}\right)^{1/2} a \tag{11}$$

This follows from the fact that the radial variation of pressure within the jet and within the melt flow are the same [compare Equation (8) with (10)]. The temperature profiles are conveniently described in terms of the following dimensionless choice:

$$\theta = \frac{T(\eta) - T_{mp}}{T_\infty - T_{mp}}, \quad \theta_m = \frac{T_m(\eta_m) - T_{mp}}{T_\infty - T_{mp}} \tag{12}$$

After substitution of Equations (7) to (12) into the partial differential equations, we obtain

$$f''' + ff'' + \tfrac{1}{2}(1 - f'^2) = 0, \quad F' = 4(ff' + f'') \tag{13}$$

$$\theta'' + Prf\theta' = 0 \tag{14}$$

for the jet region and

$$f_m''' + f_m f_m'' + \tfrac{1}{2}(1 - f_m'^2) = 0, \quad F_m' = 4(f_m f_m' + f_m'') \tag{15}$$

$$\theta_m'' + Pr_m f_m \theta_m' = 0 \tag{16}$$

for the melt region. Primes denote differentiation with respect to η or η_m. Pr (or Pr_m) is the liquid Prandtl number. It is not necessary to evaluate the functions $F(\eta)$ or $F_m(\eta_m)$ unless the pressure distribution within the flow field is required.

The boundary conditions (1), (3) to (6) may be rephrased as

$$\text{at } \eta \to \infty: \quad f' \to 1.0, \quad \theta \to 1.0 \tag{17}$$

$$\text{at } \eta_m = 0: \quad f_m' = 0, \quad f_m = -\frac{V_m}{\sqrt{2a_m\nu_m}}, \quad \theta_m = 0 \tag{18}$$

$$\theta_m' = -\frac{Pr_m}{B} f_m \tag{19}$$

at $\eta_m = \eta_\delta$ or $\eta = 0$*: $f' = \epsilon f_m'$,

$$f = f_m = 0, \quad \theta = \theta_m = \theta_i \tag{20}$$

$$f'' = A f_m'', \quad \theta' = b\theta_m' \tag{21}$$

where

$$B \equiv \frac{c_m(T_\infty - T_{mp})}{L + c_s(T_{mp} - T_o)}, \quad \epsilon \equiv \sqrt{\frac{\rho}{\rho_m}} \tag{22}$$

$$A \equiv \sqrt{\left(\frac{\rho_m}{\rho}\right)^{1/2} \frac{\nu_m}{\nu}}, \quad b \equiv \frac{k_m}{k}\sqrt{\left(\frac{\rho}{\rho_m}\right)^{1/2} \frac{\nu}{\nu_m}} \tag{23}$$

are dimensionless property ratios, and $\eta_\delta \equiv \delta(2a_m/\nu_m)^{1/2}$ is the dimensionless melt film thickness.

MATHEMATICAL SOLUTION OF THE EQUATIONS

Numerical Solution

Consideration is first given to the momentum Equations (13) and (15), and a dimensionless melting velocity $f_m(0)$ is selected. Then a guess is made for the dimensionless shear stress at the melting surface $f_m''(0)$. These values, together with the condition $f_m'(0) = 0$, provide three boundary conditions for the melt film momentum Equation (15). With these conditions, Equation (15) is integrated in the positive η_m direction to the location where $f_m = 0$. This location corresponds to the jet-film interface (that is, $\eta_m = \eta_\delta$). The values of f_m' and f_m'' at this location can be transformed by Equations (20) and (21) into values of f' and f'' once the ratios ϵ and A are assigned. With the third condition $f = 0$, the jet momentum Equation (13) is integrated with respect to η. Finally, it remains to check whether $f'(\eta)$ approaches the asymptote $f' = 1.0$ at large η. If not, a new guess is made for $f_m''(0)$, and the entire calculation is repeated until the condition $f'(\infty) = 1.0$ is fulfilled. Once the correct value for $f_m''(0)$ is found, the solutions $f(\eta)$ and $f_m(\eta_m)$ are used as input data for the solution of the energy Equations (14) and (16). With $\theta_m'(0)$ and Pr_m specified, the melting velocity and the value of B can be evaluated from Equations (18) and (19).

For the one-component system, $\epsilon = A = b = 1.0$, and the problem reduces to that which was solved numerically by Stewart and Prober (1962) for discrete values of $f_m(0)$ and Pr. Agreement with the Stewart-Prober solutions was found to be excellent.

Approximate Solution for Thin Melt Film

If the liquid film formed from the melting solid is sufficiently thin, the film Reynolds and Peclet numbers are small so that the inertia terms in the film momentum Equation (15) and the convection term in the film energy Equation (16) can be neglected, and we obtain

$$f_m''' = -\tfrac{1}{2}, \quad \theta_m'' = 0 \tag{24}$$

Integrating Equations (24) and using the boundary conditions (18) to (21), we obtain a cubic equation for the film thickness η_δ

$$\frac{1}{6}\eta_\delta^3 + \frac{f''(0)}{2A}\eta_\delta^2 = \frac{B}{Pr_m b}\theta'(0) = -f_m(0) \tag{25}$$

and we obtain a relation between the dimensionless film-jet interface temperature θ_i, and η_δ:

$$\theta_i = \frac{\eta_\delta}{b}\theta'(0) \tag{26}$$

where

$$\theta_i \equiv \frac{T_i - T_{mp}}{T_\infty - T_{mp}} \tag{27}$$

It remains to determine both the shear stress $f''(0)$ and the temperature gradient $\theta'(0)$ at the melt film-jet interface. Since the melt film is extremely thin, the radial velocity component at the interface $u_m(r, \delta) << u_\infty$ [or $\epsilon f_m'(\eta_\delta) << 1.0$]; therefore, the film acts as a solid wall as far as the oncoming jet is concerned. In this limit, the flow pattern in the jet is given, approximately, by the solution of Equation (13) with $f'(0) = 0$. The value of $f''(0)$ can be taken directly from this solution, namely, $f''(0) = 0.9277$. In order to obtain $\theta'(0)$, it will be useful to define the dimensionless temperature function

$$\Pi(\eta) = \frac{\theta(\eta) - \theta_i}{1 - \theta_i} \tag{28}$$

We note that $\Pi(\eta)$ is a solution of the energy Equation (14) and satisfies the boundary conditions $\Pi(0) = 0$ and $\Pi(\infty) = 1.0$; it is the well-known temperature profile within a stagnation flow over a nonmelting surface. Then

$$\theta'(0) = (1 - \theta_i)\Pi'(0) \tag{29}$$

$\Pi'(0)$ is the temperature gradient in the absence of melting and is a function of the jet Prandtl number only. Values of $\Pi'(0)$ have been generated, for example, by Stewart and Prober (1962). The following formula may be used with less than 5.0% error when $Pr > 1.0$:

$$\Pi'(0) = 0.553\, Pr^{1/3} \tag{30}$$

It will prove convenient to define the following additional dimensionless groups:

$$y \equiv \frac{\Pi'(0)}{b}\eta_\delta; \quad \text{(film thickness number)} \tag{31}$$

$$X \equiv \left[\frac{\Pi'(0)}{b}\right]^3 \frac{AB}{Pr_m}; \quad \text{(jet temperature number)} \tag{32}$$

$$Y \equiv -\sqrt{2}A\left[\frac{\Pi'(0)}{b}\right]^2 f_m(0); \quad \text{(melting rate number)} \tag{33}$$

Then, from Equations (25), (26), and (29), we obtain the expressions for jet temperature and melting velocity:

$$f''(0)y^2\left[1 + \frac{1}{3}\frac{Aby}{\Pi'(0)f''(0)}\right] = \frac{2X}{1+y} = \sqrt{2}Y \tag{34}$$

For many cases of interest, the quantity $Aby/[3\Pi'(0)f''(0)] << 1.0$, and it can be neglected in Equation (34). This is equivalent to assuming a linear velocity profile in the melt film, an assumption made by Roberts (1958) in his analysis. The same assumption will be made here. The elimination of y in Equation (34) results in an implicit expression that relates melting velocity Y to jet temperature X, assuming a thin melt film:

$$X = \frac{Y}{\sqrt{2}}\left[1 + \left(\frac{\sqrt{2}Y}{f''(0)}\right)^{1/2}\right] \tag{35}$$

The expression for the dimensionless melt film thickness

* For convenience we choose $\eta = 0$ at the jet-film interface. This is permissible because η does not enter into the boundary conditions.

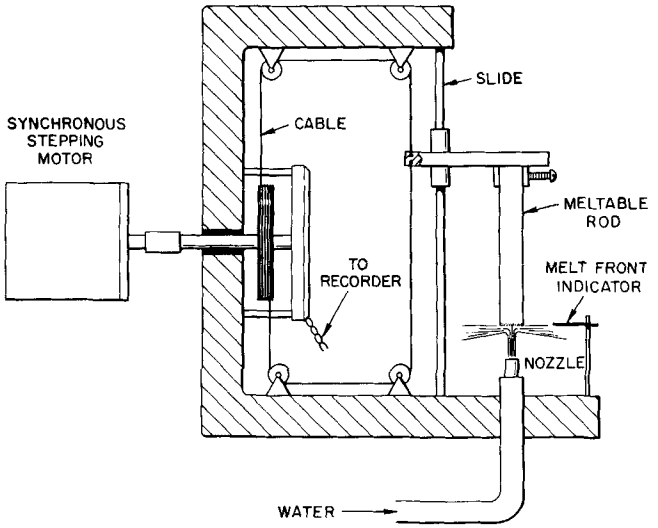

Fig. 2. Schematic diagram of the experimental apparatus.

in inverted form follows from the left side of Equation (34):

$$X = \tfrac{1}{2} f''(0)(1 + y)y^2 \tag{36}$$

Finally, from Equations (26) and (29), the interface temperature θ_i may be related to the film thickness by

$$\theta_i = \frac{y}{1 + y} \tag{37}$$

EXPERIMENTAL INVESTIGATION

The experimental apparatus is shown in Figure 2. Water from a large constant temperature reservoir is passed through a nozzle to produce a jet that is directed upward against the lower end of a meltable rod, having a diameter about twice that of the nozzle. The meltable rod is held in a sliding fixture, so that its vertical position is adjustable through the action of a high tension cable. The movement of the cable is controlled with a variable speed electric motor. The jet is deflected by the melting impingement surface, thereby setting up a flow of liquid normal to the jet that spreads radially outwards. A thin plate, which serves as a melt front indicator, is located a fixed distance above the base of the apparatus by means of a support pin. During a run, the melting rod was fed into the jet at a rate such that the melt front was always in line with the melt front indicator. This method proved to be fully successful in achieving a constant separation distance between the nozzle and the melting surface.* The rod melting rates were determined with the aid of instrumentation which converts the downward rod displacement history into an electric signal that can be recorded on an electronic strip-chart recorder. Figure 3 is a copy of a typical chart record showing the rod displacement as a function of time for water impinging on a melting octane rod. The slope of the rod displacement vs. time curve corresponds to the melting rate of the rod.

The test specimens were cylindrical rods of ice (m.p. 0°C), frozen octane (m.p. −56.8°C), frozen olive oil (m.p. −6.0°C), and frozen p-xylene (m.p. 13.2°C). The rods were approximately 15 cm long and 0.95 cm in diameter. They were cast in copper tube molds sealed at one end with a cork. After filling the mold with liquid rod material, a threaded Teflon plug was inserted into the open end. This plug was cast directly into the rod and was used for holding the rod in the sliding fixture. The ice rods were frozen in a freezer maintained at −25°C. All other rods were frozen in a liquid nitrogen bath (−196°C). Once a rod was completely frozen, the mold was placed in a warm room until the rod could be withdrawn by

* Note that the melting surface in the experiment is upside down in relation to that shown in the schematic of the physical model (Figure 1).

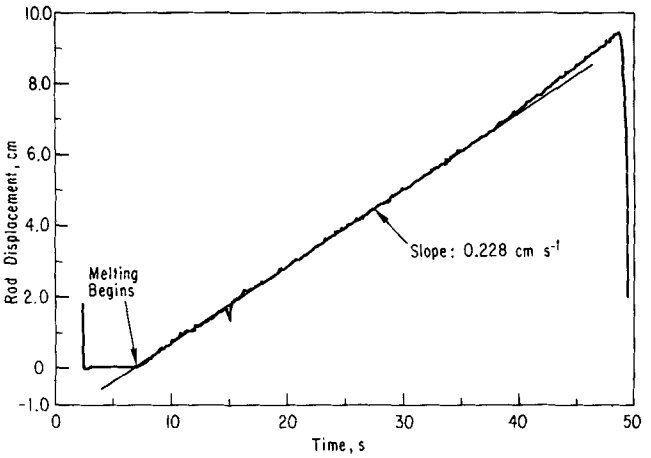

Fig. 3. Typical record of octane rod displacement. Jet velocity 1.39 m s^{-1}, jet temperature 20°C.

pulling on the Teflon plug. The rod was then returned to the cold environment for storage purposes before the initiation of an experimental run. If necessary, a warm plate was used to produce a smooth, flat surface at the end of the rod.

Two different nozzle designs were used. One of the nozzles was machined from a thick steel plug. The plug was drilled in steps of progressively smaller diameter to a final diameter of 4.76 mm. The other nozzle was simply a square edged orifice, also 4.76 mm in diameter. Within the scatter of the experimental data, the melting heat transfer data obtained with each nozzle were found to be the same. The spacing between the nozzle and the meltable rod surface was varied between 0.95 and 5.7 cm. The effect of nozzle to rod spacing on melting rates was found to be negligible over this range. All the data reported here were obtained at a nozzle to rod spacing of 2.38 cm.

After a rod was removed from the liquid nitrogen bath in preparation for a run, the rod was mounted on the apparatus and allowed to warm by convection in the air. This was done to minimize the effect of rod subcooling on measured melting rate. Preliminary tests, in which the temperature of the center of the rod was monitored as it was removed from the liquid nitrogen and placed in the fixture, showed that a minimum of about 2.5 min was required to eliminate most of the subcooling. Thus, subcooling can be neglected in the analysis of the data.

RESULTS AND DISCUSSION

The melting rate measurements were restricted to the stagnation region of the impinging jet. That is, the jet boundary-layer thickness, the melt film thickness, and

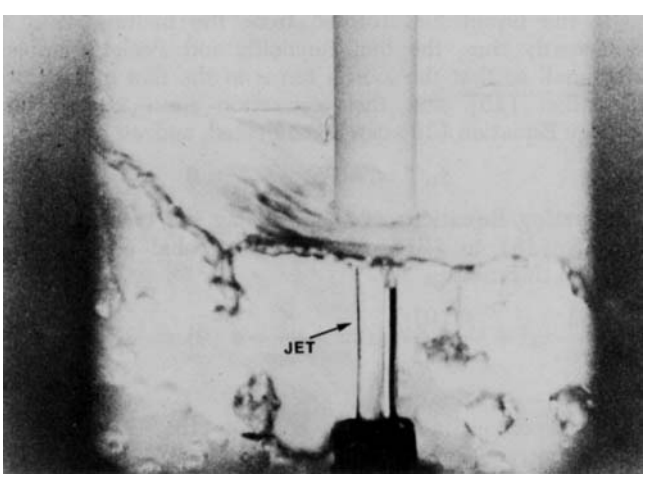

Fig. 4. Photograph of water jet impinging on the lower end of a melting octane rod.

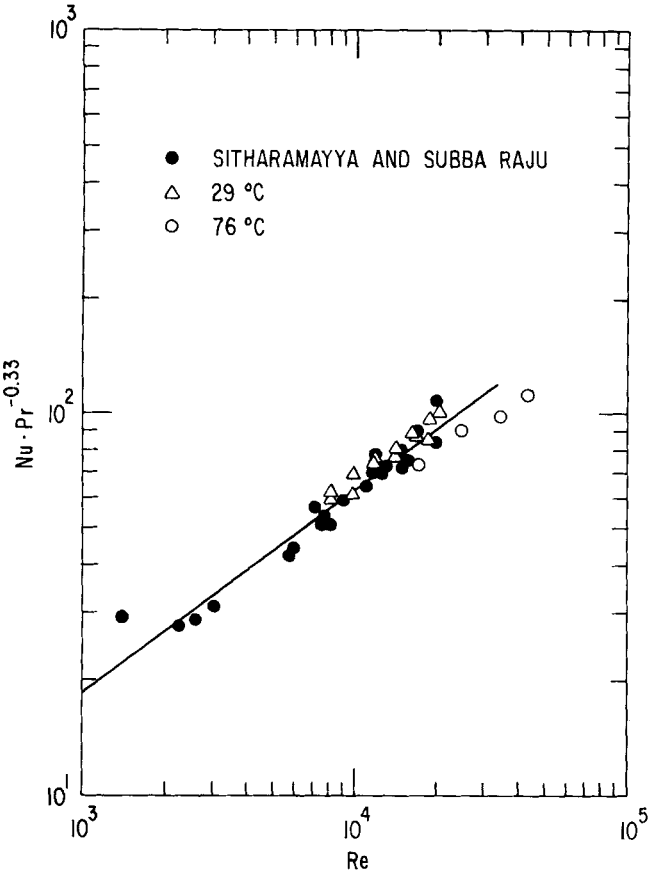

Fig. 5. Comparison of ice melting data with data of Sitharamayya and Subba Raju.

the rate of heat transfer from the jet to the melting surface were independent of the radial distance r. This was verified experimentally, since a flat liquid fan, spreading radially outward from the zone of impingement, was maintained during rod melting (see Figure 4). This indicated a flat melting front throughout the run, a situation that could only exist if heat transfer to the lower end of the rod were uniform.

Rod melting rates were measured for values of jet velocity from 1.39 to 3.52 m s^{-1} and for jet temperature from 1.0° to 80.0°C.

One-Component (Water-Ice) System

The one-component system is useful in examining jet impingement heat transfer in general. Since subcooling in the melting rod is negligible, all of the heat transferred from the jet to the rod is applied to melting the rod, and a convective heat transfer coefficient h can be obtained from the energy balance at the melting surface:

$$\rho_s L V_m = h(T_\infty - T_{mp}) \tag{38}$$

Then, a Nusselt number for impingement heat transfer with melting can be defined:

$$Nu_m = \frac{hd}{k} \tag{39}$$

The Nusselt number in this case, Nu_m, is expected to be somewhat below that for a jet impinging on a nonmelting surface Nu owing to the insulating effect of the melt film. A correction, based on the solutions for heat transfer with melting developed above, can be applied to the Nusselt number to account for the presence of the melt film. In general, however, it has been demonstrated by Epstein (1975) that the simple expression

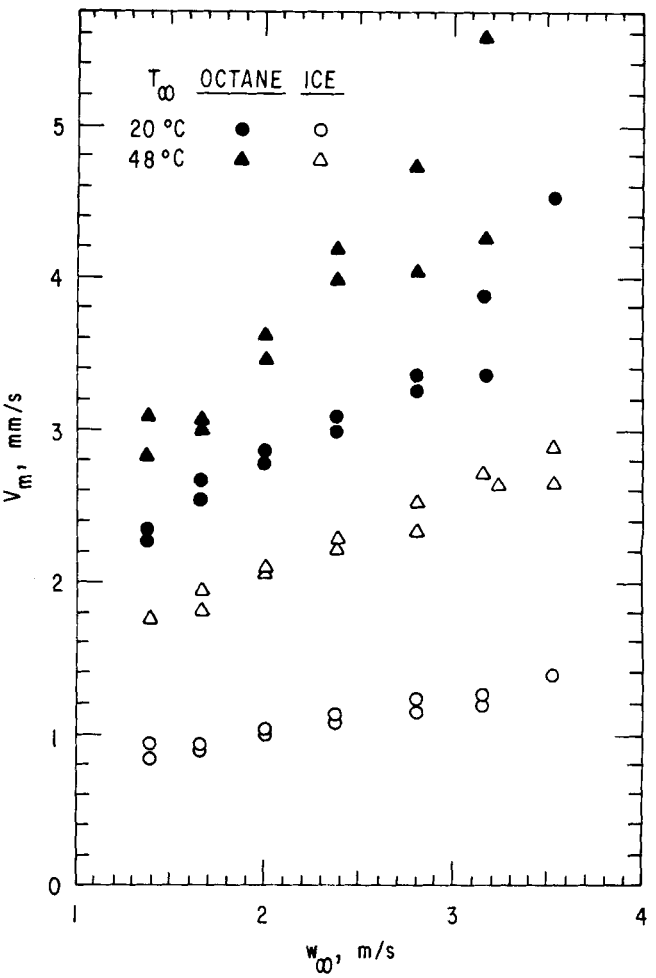

Fig. 6. Comparison of ice and octane rod melting rates.

$$Nu = \frac{B}{\ln(1+B)} Nu_m \tag{40}$$

accurately relates nonmelting to melting heat fluxes in all circumstances involving the melting of solid bodies immersed in flows of warmer fluid of the same material, where B is given by Equation (22).

With Equations (38) to (40), the melting rate data obtained for the one-component system can be compared directly to data for impingement heat transfer to a nonmelting surface. Figure 5 compares the heat transfer data for the water jet-ice rod system with that of Sitharamayya and Subba Raju (1969) for a water jet cooling a surface which is heated by steam condensing on the other side.* Melting ice rod data at two jet temperatures (29.0° and 76.0°C) are included in Figure 5, along with the correlation provided by Sitharamayya and Subba Raju for their impingement region data:

$$NuPr^{-0.33} = 0.5077\, Re^{0.523} \tag{41}$$

The good agreement is a clear indication that melting rate measurements can be used to delineate heat transfer rates for liquid jets impinging on nonmelting surfaces. The advantage of the present method is its simplicity. Where heat transfer information for the impingement region is desired, measurement of melting rate is less difficult than the temperature measurements required

* Although not specified in their report, it could be estimated that the temperature drop in their jet boundary layer varied from 30.0° to 80.0°C.

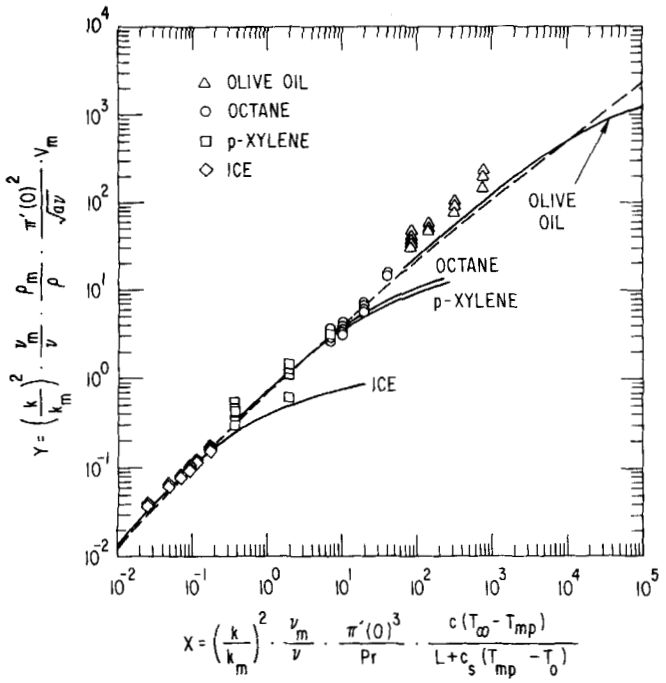

Fig. 7. Comparison of predictions with experiment. Thin film approximation – – –, exact (numerical) solution ———.

with, say, the steam condensation technique. In addition, the Sitharamayya and Subba Raju experiment required 2 hr to reach steady state conditions, whereas steady state melting conditions were achieved after a short initial transient lasting ~2.0 s.

Two-Component System

Figure 6 shows a comparison of ice rod and octane rod melting rates vs. jet velocity for two jet temperatures. The measured octane melting rate $V_{m,oct}$ is seen to be about a factor of 2.0 greater than the ice melting rate, $V_{m,ice}$. However, if the heat transport process in the water jet were identical for both the ice and octane impingement surface, a larger melting rate ratio would be anticipated, namely

$$\frac{V_{m,oct}}{V_{m,ice}} = \frac{[(T_\infty - T_{mp})/L]_{ice}}{[(T_\infty - T_{mp})/L]_{oct}} = 8.6 \qquad (42)$$

for a water jet temperature of 20°C. The observed lower melting velocity ratio simply illustrates the protective nature of the octane film. A similar behavior was observed for *p*-xylene and olive oil.

Comparison with Theory

The thin film approximation suggests the plot of dimensionless melting rate Y vs. dimensionless jet temperature X shown in Figure 7. It can be demonstrated that the expressions for X and Y [Equations (32) and (33)] can be replaced with equivalent dimensionless groups, namely

$$X = \left(\frac{k}{k_m}\right)^2 \cdot \frac{\nu_m}{\nu} \cdot \frac{\Pi'(0)^3}{Pr} \cdot \frac{c(T_\infty - T_{mp})}{L + c_s(T_{mp} - T_o)} \qquad (43)$$

and

$$Y = \left(\frac{k}{k_m}\right)^2 \cdot \frac{\nu_m}{\nu} \cdot \frac{\rho_m}{\rho} \Pi'(0)^2 \frac{V_m}{\sqrt{a\nu}} \qquad (44)$$

which contain only physical properties or quantities that have been determined in the experimental investigation.*

* It should be noted that since subcooling in the meltable rods was negligible, the term $c_s(T_{mp} - T_o)$ is taken to be zero.

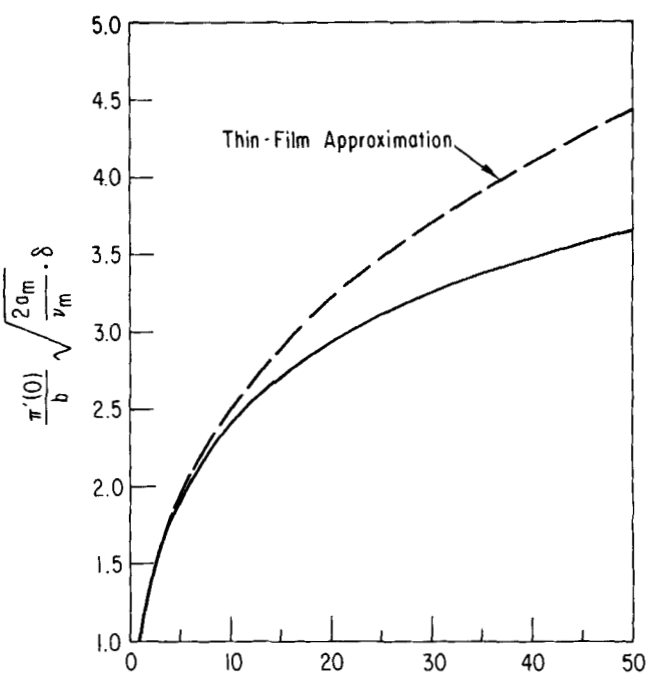

Fig. 8. Dimensionless melt film thickness vs. dimensionless jet temperature, octane.

In order to make allowance for the variation of physical properties with temperature in both the melt layer and jet, values for density, kinematic viscosity, thermal conductivity, and Prandtl number are evaluated at the average melt film temperature $\frac{1}{2}(T_i + T_{mp})$ and at the average jet boundary-layer temperature $\frac{1}{2}(T_i + T_\infty)$.

In the figure, experimental results are compared with the exact solutions (dark curves) as well as with the

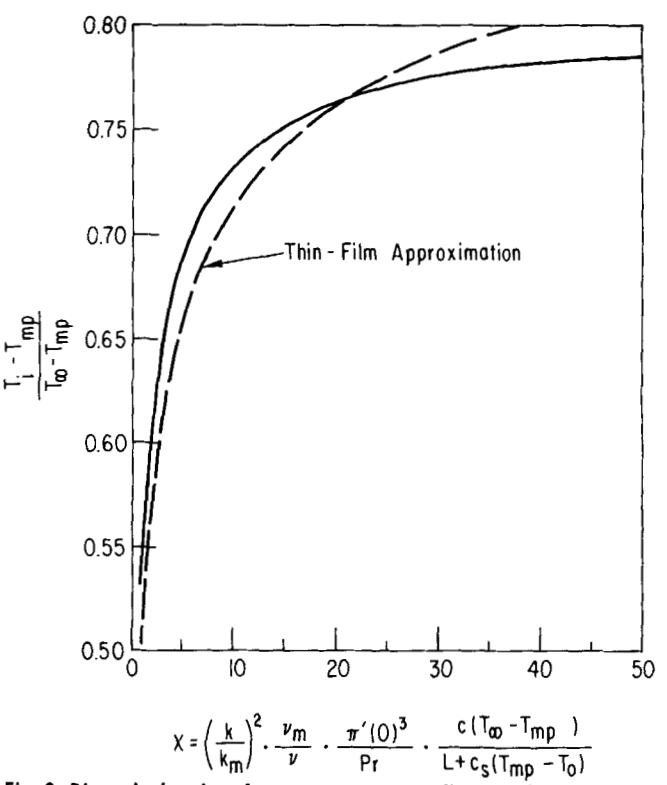

Fig. 9. Dimensionless interface temperature vs. dimensionless jet temperature, octane.

thin film approximation (dashed curve). Note that the thin film solution is universal, applying to any combination of solid and jet materials. The exact solutions are seen to predict lower melting rates than the approximation at higher jet temperatures. This is to be expected, since the melting velocity acts to reduce the steepness of the temperature gradient at the melting surface, thereby providing a lower driving force for melting than predicted by the thin film approximation. Note that the thin film approximation underestimates the melting rate for olive oil. The assumption of a linear velocity profile in the melt layer breaks down at large values of X, and it becomes necessary to deal with the more general form of the thin film approximation [namely, Equation (34)].

Both the thin film solution and the exact solutions show good agreement with all data, excepting olive oil, where a significant error is observed. It is believed that the large variation in viscosity with temperature for olive oil is responsible for this error. It is interesting to note that the thin film solution accurately predicts melting rates over the range of jet temperatures used in the experimental investigation. Apparently the temperature difference that drives the melting process must be quite large before inertia and convection effects in the melt film become important.*

Melt Film Thickness and Interface Temperature

Plots of dimensionless film thickness and interface temperature vs. X for octane are shown in Figures 8 and 9. Exact solutions are compared with values calculated using the thin film approximation. The curves indicate the general behavior of these quantities with increasing jet temperature, as well as the relative error associated with the thin film approximation. From Figure 8 we predict a melt film thickness δ of 0.02 to 0.03 mm over the range of jet temperatures employed in the experiment. Figure 9 indicates that even at low jet temperatures T_∞, most of the temperature drop occurs in the octane melt layer. From Figure 9 we predict an interface temperature T_i in the range 0° to 30°C for jet temperatures $15 < T_\infty < 80$°C. Interestingly enough, if the jet temperature falls below 15°C, an ice layer is predicted to form at the octane melt-water jet interface. Experimental observations of such ice layers were made in a laboratory study of simultaneous melting and freezing in the impingement region of a liquid jet described elsewhere (Epstein et al., 1978).

ACKNOWLEDGMENT

Thanks are due to Kathy Cummings for an excellent job of typing the manuscript. This work was performed under the auspices of the U.S. Department of Energy and is based in part on a dissertation submitted to the faculty of Marquette University by M. J. Swedish in partial fulfillment of the degree of Master of Science.

NOTATION

a = stagnation point velocity gradient, w_∞/d
a_m = stagnation point velocity gradient for melt film, Equation (11)
A = dimensionless property ratio, Equation (23)
b = dimensionless property ratio, Equation (23)
B = melting parameter, Equation (22)
c = heat capacity
d = diameter of nozzle
f = dimensionless similarity velocity variable
F = dimensionless similarity pressure variable
h = convective heat transfer coefficient
k = thermal conductivity
L = latent heat of fusion of the melting solid material
Nu = Nusselt number with no melting, Equation (40)
Nu_m = Nusselt number with melting, Equation (39)
P = fluid pressure
P_o = fluid pressure at stagnation point
Pr = Prandtl number
r = radial coordinate
Re = jet Reynolds number evaluated at the nozzle exit
T = temperature
T_{mp} = melting point of solid material
T_o = temperature in the solid at a large distance from the melting surface
u = velocity component in r direction
V_m = melting velocity
w = velocity component in z direction
X = jet temperature number, Equation (32) or (43)
y = film thickness number, Equation (31)
Y = melting rate number, Equation (33) or (44)
z = coordinate perpendicular to melting surface

Greek Letters

α = thermal diffusivity
δ = melt film thickness
η = dimensionless similarity coordinate, Equations (7) and (9)
η_δ = dimensionless melt film thickness $\delta(2a_m/\nu_m)^{1/2}$
θ = dimensionless temperature, Equation (12)
μ = absolute viscosity
ν = kinematic viscosity
Π = dimensionless temperature solution in the absence of melting, Equation (28)
ρ = density

Subscripts

i = at the melt film jet interface
m = melt film
s = solid material
∞ = at the nozzle or in the free stream

LITERATURE CITED

Donaldson, C. D., R. S. Snedeker, and D. P. Margolis, "A Study of Free Jet Impingement. Part 2. Free Jet Turbulent Structure and Impingement Heat Transfer," *J. Fluid Mech.*, **45**, 477 (1971).

Epstein, M., "The Effect of Melting on Heat Transfer to Submerged Bodies," *Letters in Heat Mass Transfer*, **2**, 97 (1975).

———, M. J. Swedish, J. H. Linehan, G. A. Lambert, G. M. Hauser, and L. J. Stachyra, "Simultaneous Melting and Freezing in the Impingement Region of a Liquid Jet," paper presented at the Winter Annual ASME Meeting, San Francisco, Calif. (Dec., 1978).

Erickson, G. G., and D. B. Olfe, "Growth and Decay of Perturbations at an Interface in a Stagnation Counterflow," *J. Fluid Mech.*, **84**, 401 (1978).

Gilpin, R. R., "The Ablation of Ice by a Water Jet," *Trans. Can. Soc. Mech. Engrs.*, **2**, 91 (1973).

Giralt, F., C. J. Chia, and O. Trauss, "Characterization of the Impingement Region in an Axisymmetric Turbulent Jet," *Ind. Eng. Chem. Fundamentals*, **16**, 21 (1977).

Lipsett, A. W., and R. R. Gilpin, "Laminar Jet Impingement Heat Transfer Including the Effects of Melting," *Intern. J. Heat Mass Transfer*, **21**, 25 (1978).

Martin, H., "Heat and Mass Transfer between Impinging Gas Jets and Solid Surfaces," in *Advances in Heat Transfer*, Vol. 13, p. 1, Academic Press, New York (1977).

Mellor, M., "Cutting Ice With Continuous Jets," Second International Symposium on Jet Cutting Technology, Cambridge (Apr. 2-4, 1974).

* Deviations from thin film behavior are due mainly to convection (or temperature profile distortion) when $Pr_m > 1.0$.

Roberts, A. L., "On the Melting of a Semi-Infinite Body Placed in a Warm Stream of Air," *J. Fluid Mech.*, 4, 505 (1958).
Savino, J. M., J. F. Zumdieck, and R. Siegel, "Experimental Study of Freezing and Melting of Flowing Warm Water at a Stagnation Point on a Cold Plate," Fourth Int. Heat Transfer Conference, Paris-Versailles, 1, Cu 2.10 (1970).
Sitharamayya, S., and K. Subba Raju, "Heat Transfer Between an Axisymmetric Jet and a Plate Held Normal to the Flow," *Can. J. Chem. Eng.*, 47, 365 (1969).
Stewart, W. E., and R. Prober, "Heat Transfer and Diffusion in Wedge Flows with Rapid Mass Transfer," *Intern. J. Heat Mass Transfer*, 5, 1149 (1962).
Yang, K. T., "Formation of Ice in Plane Stagnation Flow," *Appl. Sci. Res.*, 17, 377 (1966).
Yen, Y. C., and A. Zehnder, "Melting Heat Transfer with Water Jet," *Intern. J. Heat Mass Transfer*, 16, 219 (1973).

Manuscript received September 26, 1978; revision received February 12 and accepted February 20, 1979.

Flow Through Tubes with Sinusoidal Axial Variations in Diameter

J. A. DEIBER
and
W. R. SCHOWALTER
Department of Chemical Engineering
Princeton University
Princeton, New Jersey 08540

An iteration technique has been developed to solve the equations of motion for flow of an incompressible Newtonian fluid through a circular tube with a radius which varies sinusoidally in the axial direction. The iteration is essentially geometric; one proceeds from a solution for flow through a tube in which the wavelength of diameter change in the axial direction is arbitrarily large to a solution for the wavelength and amplitude of interest. Theoretical predictions of inception of secondary flow are in good agreement with experiments.

SCOPE

Several solutions now exist for flow of Newtonian fluids through tubes with axial periodic variations in diameter. These range from finite-difference solutions of the Navier-Stokes equation for flow through tubes with cusp shaped walls to solutions of the creeping flow equation for flow through tubes with sinusoidally varying diameter. The results are believed to be representative of the flow, under certain conditions, in packed beds and in porous rock. Thus, the work pertains to heat and mass transfer problems in packed beds and to questions associated with secondary and tertiary recovery of petroleum.

It was our desire to provide both computational and experimental results for flow in a circular tube with sinusoidal axial variations in diameter. Chow and Soda (1972) have solved the problem analytically over a limited range of parameters, and Fedkiw and Newman (1977) used a collocation method for the same geometry in the creeping flow regime. The computations presented here remain valid beyond the point where inertial effects are negligible. A new iteration technique was used in which the problem is first solved for a tube wavelength such that locally Poiseuille flow obtains. The wavelength was then decreased by suitably small decrements until a solution was found for the wavelength of interest. The method was found to be economical in terms of computer time.

Experiments were conducted in a tube with an amplitude of radial oscillation equal to 0.3 cm and a wavelength of 6.28 cm. The average tube radius was 1 cm. Pressure drop was measured with conventional pressure taps, and streamlines, including secondary vortices, were observed with a polystyrene latex tracer suspension.

CONCLUSIONS AND SIGNIFICANCE

By iteration from a geometry with a weakly varying axial change in diameter to one in which the change with axial distance is appreciable, one can readily calculate laminar velocity profiles for flow through tubes with variations from the mean diameter which approximate 0.6. Results can be obtained for conditions in which inertial effects are important.

The computations are in good agreement with experimental determinations of friction factor as a function of Reynolds number. The agreement holds beyond the Reynolds number at which inertial effects are important. The shape of a secondary toroidal vortex, which appears as a consequence of inertia, is accurately predicted.

The computational method is attractive because of its relative simplicity and because it can readily be extended to nonlinear equations, such as those which describe the flow of non-Newtonian fluids.